University of New Haven

Digital Commons @ New Haven

Master's Theses   Student Works

5-2020

Non-PLL Direct Power Control for a Single-Phase Grid-Connected Three-Level Inverter

King Ademola Adebo

Follow this and additional works at: https://digitalcommons.newhaven.edu/masterstheses

Part of the Electrical and Computer Engineering Commons

THE UNIVERSITY OF NEW HAVEN

TAGLIATELA COLLEGE OF ENGINEERING

Department of Electrical & Computer Engineering and Computer Science

Non-PLL Direct Power Control for a Single-Phase Grid-Connected Three-Level Inverter

A THESIS

Submitted in partial fulfilment of the requirements for the degree of

MASTER OF SCIENCE IN ELECTRICAL ENGINEERING

BY

King Ademola Adebo

University of New Haven,

West Haven, Connecticut,

May 2020

Non-PLL Direct Power Control for a Single-Phase Grid-Connected Three-Level Inverter
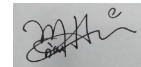
APPROVED BY

_____

[Junhui Zhao, Ph.D.]
Thesis Adviser

_____

[Ali Golbazi, Ph.D.]
Committee Member

_____

[Mohsen Sarraf, Ph.D.]
Committee Member

_____

[Bhuiyan, Md Moinuddin, Ph.D]
Committee Member

_____

[Ali Golbazi, Ph.D.]
Department Chairperson

_____

[Ali Golbazi, Ph.D.]
Director of the Graduate Program

_____

[Ronald S. Harichandran, Ph.D.]
Dean of Tagliatela College of Engineering

_____

[Mario Thomas Gaboury Ph.D.]
Provost

DEDICATION

This thesis is dedicated to my parents. The limitless support you provided made this possible.

ACKNOWLEDGEMENTS

Abstract

The growing demand for clean, reliable renewable energy generation has led to the widespread adoption of solar energy as a source of electricity. Technological advancement aiding to reduce the cost of solar photovoltaic (PV) panels, as well as improvement in power electronics and control strategies for solar PV systems have also contributed to the growing popularity. For grid-connected solar systems to adequately meet future demand and grid requirements, the system must be reliable, and not affected by instability or distortions on the power grid.

In this thesis, a control strategy for single-phase grid-connected inverters that can synchronize to the grid without a phase lock loop (PLL) is proposed. The PLL is an important device that is relied on for the synchronization of solar PV systems to the electrical grid. However, the PLL has an inherently complex design and its performance is often negatively affected if the grid voltage has poor quality. In addition, eliminating the use of PLL for synchronization can avoid the issue of slow dynamic response, higher harmonics, and increased computation complexity.

The real and reactive power of the single-phase, three-level neutral point clamped (NPC) inverter is controlled by using a direct power control (DPC) strategy. A novel method of computing the power components of the single-phase inverter is proposed and this technique further improves the precision of the power components calculated by compensating the frequency and phase deviation compensation. Finally, simulations are carried out by using MATLAB/Simulink to demonstrate the effectiveness of the proposed methodology.

Contents

Table of Figures

Table of Tables

CHAPTER 1: INTRODUCTION

1.1 Background of Study

To date, the energy demand of the U.S. has been largely met by centralized plants powered by fossil fuels. The relatively low cost of natural gas, the availability of established synchronous generation technology, as well as the flexibility of these legacy systems are reasons why fossils fuels still account for 62.7% of the total electricity generated [1]. However, the continued reliance on fossil fuels for the generation of electricity has raised serious environmental concerns causing the government to place more emphasis on integrating renewable energy sources such as wind and solar to the electrical grid on a large scale. Most states in the U.S. are required to have a significant portion of their electricity generated from renewable energy sources and some states offer rebates and incentives for efforts geared towards clean energy adoption [2].

This effort, so far, has led to the increased penetration of renewable energy sources. From 2009 to 2019, the net electricity generation using solar as the primary energy source has increased from 891,000 MWh to 107,275,000 MWh. The success recorded with solar energy adoption can be attributed to several factors, such as the financial incentives offered, growing climate concerns, and advancement in technology. The growing popularity of solar energy for electricity generation has also led to increased adoption of distributed generation (DG). DG refers to the generation of electrical energy on a small scale close to the load center. The common source of energy includes solar, wind, and fuel cells. The goal of DG is to provide alternatives to conventional power sources such as natural gas and coal. Because of the close proximity of the generation source to the load, DGs are efficient and have low emissions. As well as serving as an alternative, DGs can enhance the reliability of the grid, improve power quality, and reduce transmission losses when used with conventional energy sources.

Over the years, especially in developing countries, solar PV systems have been predominantly used with batteries in a standalone setup. In this arrangement, the PV system harnesses sunlight during the daytime and relies on the battery to power the home when there is no irradiation. However, grid-connected PV systems are now gaining prominence. This configuration facilitates the supply of electricity from the PV system to the grid. When solar irradiance peaks, the excess energy can then be fed to other customers, further reducing the reliance on conventional sources. Single-phase converters are used to integrate with single-phase distribution network for bi-directional power flow and ease of power control. As grid-connected PV systems gain prominence, strict adherence to standard regulations must be ensured. Power quality, current harmonics, and voltage deviation are factors that can be used to determine the performance and these factors are relied upon in this study.

This thesis explores different control strategies, as well as modulation schemes for single-phase grid-connected PV converters. A novel grid synchronization strategy will be proposed, and accurate power calculation can be realized by using the technique presented.

1.2 Thesis Contribution

Generally, there are two categories of control strategies for power converters: the first is direct current control, and the second is direct power control. Examples that fall under direct current control include reference frame current control, instantaneous current control, and predictive current control. The direct power control strategy (DPC) for the single-phase, three-level inverter is used in this thesis. The novelty of this thesis is the elimination of commonly used component; the phase locked loop (PLL) for synchronization. This thesis proposes frequency-based methods for the synchronization of the inverter to the grid.

1.3 Literature Review

Due to the complexity of the electrical grid, it is necessary to continuously and instantaneously monitor the state of the grid variables. This is why the three-phase instantaneous power theory is desirable because even without a synchronizing unit, the information required for synchronization can be computed. However, in a single-phase system, the control schemes based on this theory are not applicable. This is because, in comparison with the three-phase power theory, there is no similar power calculation method that computes the real and reactive power components for a single-phase system. Also, the orthogonal vector in a single-phase system required for the coordinate transformation is not easily computed. This led to the development of techniques suitable for orthogonal vector estimation in single-phase systems such as the 90-degree phase delay method, the second order generalized integration (SOGI) method, and the Hilbert transformation method [3–5].

Single-phase converters have become widely popular in recent times, and their application is widespread, ranging from grid-connected PV systems and motor drives to uninterrupted power supply (UPS) systems. They offer advantages like low current harmonics, low $\frac{dv}{dt}$, as well as the bidirectional flow of energy. The need for a smart grid with a well-diversified mix of both renewable energy sources and fossil fuels has increased the adoption of solar PV systems and wind turbine systems for energy generation. This increase in adoption is also fueled by the reduced cost of solar panels worldwide. The calculation of instantaneous power in single phase systems relies on the accurate detection of the grid information. Similarly, control schemes like voltage-oriented control, instantaneous current control, and direct power control (DPC) all rely on the accuracy of the grid detection and grid synchronization methods.

The strategies used for synchronizing the inverter to the grid are broadly classified into two. The first class is the frequency-domain detection method and we also have the time-domain detection method. One of the most common techniques used for grid monitoring and grid synchronization is the phase-locked loop (PLL), and this is a time-domain detection method [6]. Essentially, the PLL consists of several components namely

1. The phase detector (PD),

2. A loop filter (LF), and

3. A voltage-controlled oscillator (VCO).

The PLL is a feedback control system whereby the output of the PD is equal to the difference between the phase angle of the input signal and the output of the VCO. LF is a low-pass filter which eliminates the AC components [7].

Even though the PLL method of synchronizing a power converter to the electrical grid is the most widely acknowledged method, it is not without drawbacks. The degraded performance when there's unbalanced grid voltage, frequency deviation, or harmonics, due to the high sensitivity to phase angle deviation makes it undesirable [8-10].

This paper adequately covers the DPC strategy, which incorporates the proportional-integral (PI) controllers. In section III, the technique used to synchronize the grid without using a PLL is explored. This paper concludes by carrying out simulations to examine the accuracy of the proposed method and also comparing simulation results to the expected results.

In this thesis, a novel power calculation scheme is proposed to eliminate the use of PLL. And then, the frequency and phase errors caused by the proposed method are analyzed in detail

under the condition that large frequency fluctuation and wave distortion exist in the main voltage, and a compensation matrix is presented to correct these errors.

1.4 Layout of Dissertation

The second chapter of this dissertation explores the solar PV system and its modeling. The grid-connected and standalone applications of solar PV are highlighted. The section also explores the different Maximum Power Point Tracking (MPPT) topologies available. Different single-phase inverter topologies are also researched, highlighting their advantages and disadvantages.

The third chapter provides a solid background on different methods of grid-synchronization and grid-monitoring. This section also delves into the standards and regulations required for distributed generation and integration of renewables to the grid. The most popular methods of synchronization, such as PLL, DFT, and zero-crossing method, are explained. The Fourier Series, which is the underpinning technique used in this thesis, is also explored in detail.

In the fourth chapter, the different modulation techniques used for controlling inverters are examined. We first analyze the two different control methods, voltage-oriented and current-oriented control, and eventually present the direct power control (DPC) for single-phase, grid-connected inverters. Techniques like Third Harmonic Injection Pulse Width Modulation (THPWM), Sinusoidal Pulse Width Modulation (SPWM), and Space Vector Pulse Width Modulation (SVPWM), and the effect they have on harmonics are explored. The SVPWM method used for balancing the capacitor voltage is also presented.

The fifth chapter gives an overview of a single-phase PV system connected to the electrical grid. The technique for modulation and control is presented. The simulation of the overall system

is also presented in MATLAB/Simulink, and the results are discussed. The analysis of the harmonics, as well as the system's transient response, is presented.

Chapter 6 discusses the limitations and challenges of the dissertation. The section also provides recommendations on the work done and suggests future work.

CHAPTER 2: MODEL OF A SOLAR PHOTOVOLTAIC CELL

2.1 Solar Photovoltaic PV Generation

Solar energy is an abundant renewable energy source that can be harnessed in several ways. One of the ways to utilize the irradiation of the sun is the solar thermal technology. This technology uses mirrors or other forms of reflectors to concentrate the sun's rays towards a container storing liquid, usually water. Over time, the liquid boils and is turned into steam, and the steam is used to power a turbine which is connected to a generator. Solar energy can also be used as a passive heating source to power up residential buildings. However, this thesis focuses on the technology known as solar photovoltaic (PV) generation.

The photovoltaic effect explains the conversion of solar energy to electricity. In 1839, Becquerel identified that certain materials had the ability to convert light to electrical energy and by 1954, Chapin, Fuller, and Pearson [11] fabricated the first solar cell with a 6% efficiency. Now we have solar panels with efficiency between 15% and 23%. Cells made of gallium arsenide (GaAs) have a conversion efficiency of over 30%.

2.2 Solar PV Modeling

In the absence of light, the solar cell closely models a diode in the reverse-bias mode. Under short-circuit conditions, the solar cell operates as an ideal current source. The value of this current is directly proportional to the irradiance on the cell. Because cells are usually connected in series to multiply the output voltage, it is important to make sure each cell produces identical current output for the same incident insolation and temperature.

In the circuit shown in Figure 2.1, I_L (the current source) typifies the generation of energy upon incident irradiance. A shunt diode connected in parallel defines the charge carrier

recombining at high forward-bias voltage V_d. The shunt resistor R_{sh} models the high-current path in the silicon wafer.
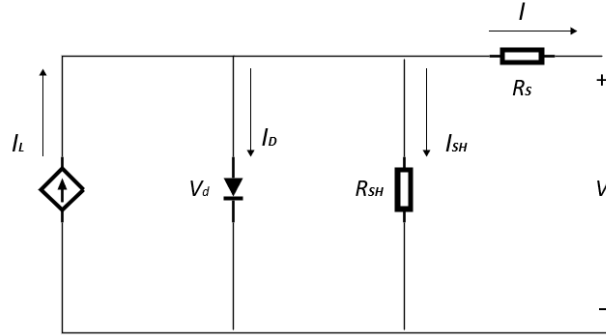
Figure 2.1:Solar PV Equivalent Circuit

The *I-V* relationship of an ideal solar PV cell is described as shown

$$I = I_l - I_D - I_{sh} \tag{2.1}$$

$$I_D = I_o \left(e^{\frac{qV}{kT}} - 1 \right) \tag{2.2}$$

$$I_{sh} = \frac{V_{PV} + IR_s}{R_{sh}} \tag{2.3}$$

And the voltage is

$$V_D = V_O + R_s I \tag{2.4}$$

$$V_T = \frac{kT}{q} Q_T n_C \tag{2.5}$$

where,

I_o is the reverse saturation current,

I_l represents the current generated by the photon,

I_D represents the diode current,

I_{sh} is the shunt current,

k stands for the Boltzmann constant which is 1.3806 x 10^{-23} JK^{-1},

$\frac{kT}{q}$ = 25.7 mV at 25°C,

n_C refers to the number of series-connected cells,

Q_T is the quality factor of the diode,

V_D is the diode voltage, and

V_T is the solar cell thermal voltage.

The relationship between the photocurrent and the intensity of incident irradiance is as shown

$$I_l = I_l(G_o)\frac{G}{G_o} \tag{2.6}$$

where,

G stands for the sunlight intensity (W/m²), and

G_o = 1000 W/m².
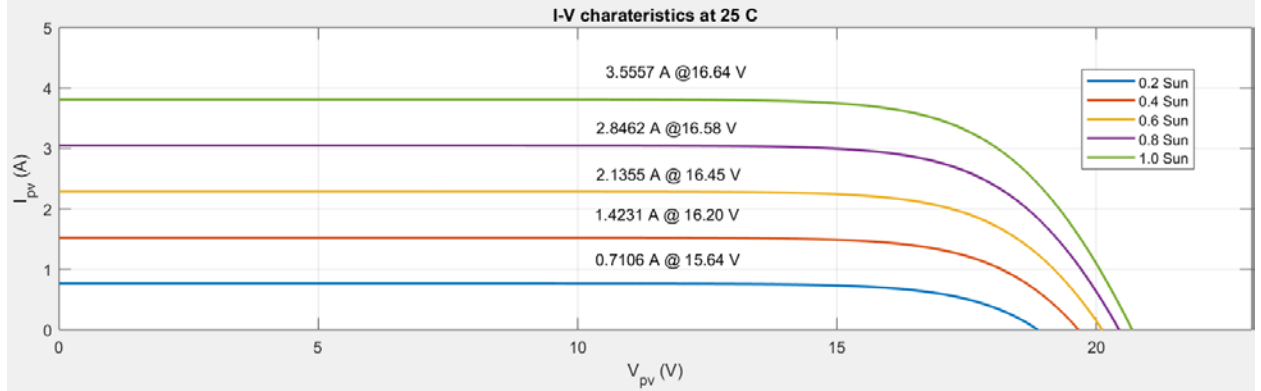
Figure 2.2: I-V characteristics of a Solar PV module with varying irradiance
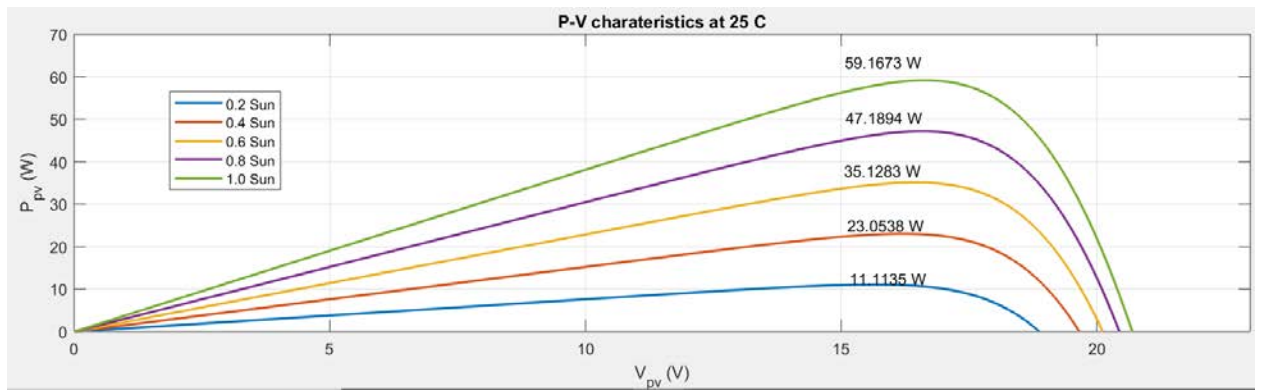
Figure 2.3: P-V characteristics of a Solar PV module with varying irradiance

Figure 2.2 presents the *I-V* curve of a solar PV module varies with incident irradiance, while Figure 2.3 shows the relationship between irradiance and the output power at 25˚C.

2.3 Fill Factor

The fill factor (FF) of a solar PV cell defines the difference between the characteristics of a practical cell and an ideal one. In essence, the fill factor measures the quality of the PV cell. This factor is expressed as

$$FF = \frac{P_{max}}{I_{sc}V_{oc}} \tag{2.7}$$

where,

22

P_{max} is the maximum power that can be generated,

I_{sc} is the short circuit current, and

V_{oc} is the open circuit voltage.

2.4 Maximum Power Point Tracking (MPPT)

Figure 2.3 shows that the power output of a solar PV system is not constant throughout the day. As the temperature changes hourly, the output power reduces or increases based on the irradiance. Because of this variation, there is a point whereby the output power is maximum, and this only occurs at certain levels of irradiance and temperature. In order to ensure that the output of this solar panel is held maximum, some algorithms have been developed. These algorithms are explored below.

2.4.1 Modified Fractional Open-Circuit Voltage (V_{OC}) Technique

Unlike the conventional fractional V_{OC} technique which leverages the linear relationship between the maximum point voltage and V_{OC} of the PV panel, the modified technique accounts for other discrepancies. The equation describing the conventional V_{OC} technique is as shown

$$V_{MP} = K \times V_{OC} \tag{2.8}$$

where,

V_{MP} is the maximum point voltage,

K is the proportionality constant,

V_{OC} is the open-circuit voltage, and

V_{OC} is measured by isolating the converter.

Even though the conventional method is cheap and easy to implement, the major drawback is that the maximum point is often not the exact value, it is an approximated one. The approximation depends on the value of K, and this value often varies. Another disadvantage is that this method requires constant isolation to measure V_{OC}, which often results in loss of power.

The conventional technique is then modified as shown

$$V_{OC} = C_{TV} C_{GV} V_{OC}^{STC} \tag{2.9}$$

$$C_{TV} = 1 + \frac{K_V}{V_{OC}^{STC}} (T - 25) \tag{2.10}$$

$$C_{GV} = 1 + \beta_T \alpha_G (G - 1000) \tag{2.11}$$

where,

C_{TV} describes how V_{OC} varies with temperature,

V_{OC}^{STC} is the open-circuit voltage at standard test conditions,

C_{GV} describes how V_{OC} varies with irradiance,

β_T and α_G are constants, and

K_V is the temperature coefficient of the open-circuit voltage.

With this modified method, it is easy to determine the maximum point voltage and a PI controller can minimize the difference between the expected maximum point voltage and the output voltage of the PV panel.

2.4.2 Perturb and Observe Method

This perturb and observe (P&O) technique involves sporadically reducing or increasing the duty cycle of the terminal voltage of the solar panel in a bid to make adjustments to the point at which the system is operating. The change in output power (ΔP) is constantly monitored as this perturbation is applied. If ΔP is positive, it implies that the maximum point is being reached, and the same perturbation applied previously is kept. If the variation is negative, the perturbation is reversed.

Requiring just two sensors, the simplicity of the P&O technique is one of the reasons why it is widely accepted. However, this method also has some significant drawbacks. One major disadvantage is that the constant perturbation causes oscillations. Even though they can be minimized by reducing the perturbation step size, the reduction affects the tracking speed.

2.4.3 Incremental Conductance Method

In this technique, dP/dV, an integral characteristic of the solar panel is used for tracking the maximum point. The solution for finding the local maximum of a differential equation also applies here, as seen in (2.12).

$$\frac{dP}{dV} = 0 = \frac{d(IV)}{dV} = I + V\frac{dI}{dV} \tag{2.12}$$

At the maximum point, we have, $\frac{dI}{dV} = \frac{-I}{V}$

where,

$\frac{I}{V}$ is the instantaneous conductance, and

$\frac{dI}{dV}$ is the incremental conductance.

25

With this MPPT algorithm, the decision to increase or decrease the duty cycle is based on the instantaneous and incremental conductance computed. Just like the P&O method, the step size results in oscillations, and minimizing the step size reduces the tracking speed. However, an advantage to the incremental conductance technique is that it offers a better transient response.

2.5 Single-Phase Inverters

The H-bridge inverter shows the most basic topology of the single-phase inverter. It is termed H-bridge because the setup of the semiconductor switches and the load parallels the letter H. As shown in Figure 2.4, the H-bridge inverter has two legs with two series-connected power switches on each leg. The load is connected in the middle of both legs, and a diode is connected in parallel to each transistor to serve as a current path when the switch is turned off. To control this inverter, the on time of the power switches on each leg is varied accordingly. One strict condition that must be met in controlling the switches is that two switches on a leg can never be on simultaneously to avoid a short circuit.
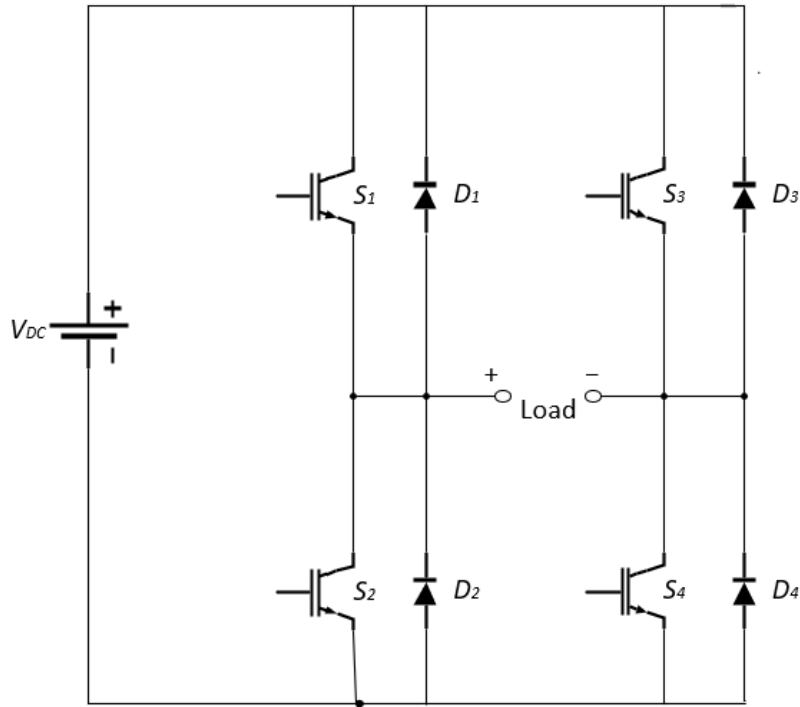
Figure 2.4: H-bridge inverter topology

The relationship between both power switches on the leg of the inverter is complementary, and this means switches S_1 and S_2, as well as S_3 and S_4 are complementary. A controller is used to achieve this variation, and there's a delay usually in nanoseconds known as *blanking time,* which avoids any overlap between the switching intervals.

The instantaneous output voltage of the inverter is either V_{dc}, -V_{dc}, or 0, as shown in Table 2.1.

Table 2.1: Switching pattern for H-bridge inverter

Switches Closed	Output Voltage
S_1 and S_2	+VDC
S_3 and S_4	−VDC
S_1 and S_3	0
S_2 and S_4	0

2.6 Multi-Level Inverters

The basic H-bridge inverter produces output voltage within V_{dc} and -V_{dc}. However, other circuits have been developed with the capacity to produce increased levels of voltage. Because of the nature of the output voltage, they are helpful in reducing harmonics and distortion. These circuits are commonly referred to as multilevel inverters, and some of the popular examples of inverters using this topology are discussed below.

2.6.1 Neutral Point Clamped (NPC) Inverter

The Neutral Point Clamped (NPC), also known as the diode-clamped (because each leg of the inverter has two diodes acting as clamps) multilevel inverter topology is one of the first practical topologies proposed. Introduced in 1980 by Nabae, et al. [12], the popularity of the NPC configuration has soared, and it has become one of the most common topologies adopted due to the reduced total harmonic distortion (THD), and reduced leakage current.

The NPC inverter has a DC voltage source connected to two series-connected capacitors. These capacitors are equally charged to $V_{dc}/2$, and the topology is shown in Figure 2.5.
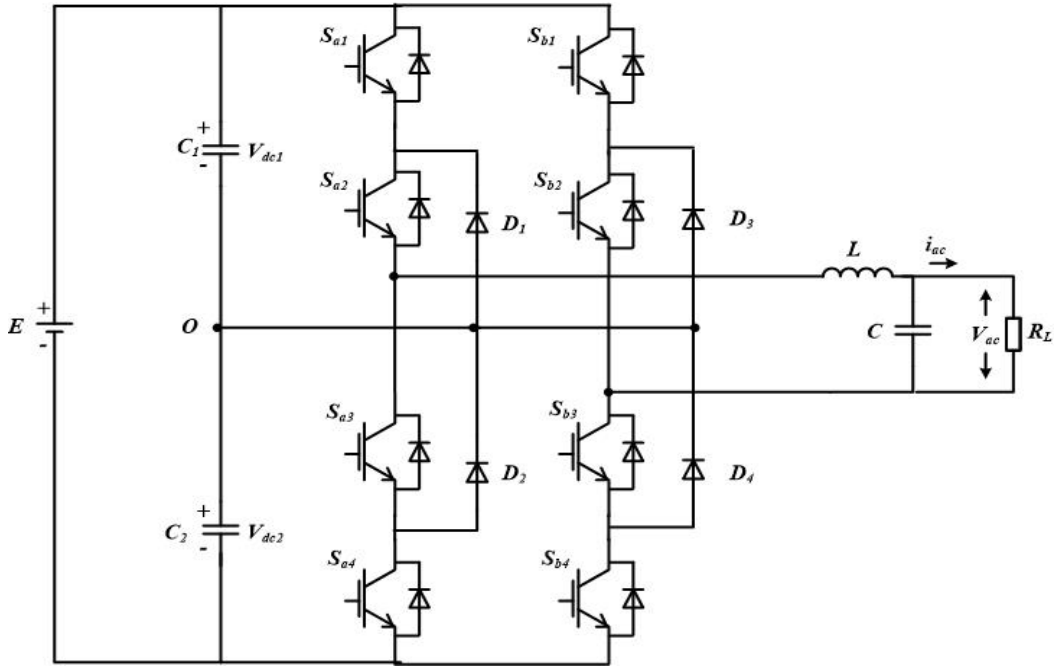
Figure 2.5: Neutral point clamped three-level inverter

Considering the first leg of the inverter, when switches S_{a1} and S_{a2} are closed, and switch S_{a3} and S_{a4} are open, the voltage across the leg is V_{dc}, and the diodes are not conducting. When S_{a1} and S_{a2} are open and S_{a3} and S_{a4} are closed, the voltage is zero. In this case, the diodes are also not conducting. For cases where S_{a2} and S_{a3} are closed and S_{a1} and S_{a4} are open, the voltage produced is $V_{dc}/2$.

The same concept applies to the second leg of the inverter. Hence, the output voltage can be calculated to give five different voltage levels.

$$v_0 = \left\{ V_{dc}, \frac{1}{2}V_{dc}, 0, -\frac{1}{2}V_{dc}, -V_{dc} \right\} \tag{2.13}$$

By using this method, it is possible to have more than five levels of the output voltage produced by adding more power switches and capacitors.

2.6.2 Cascaded H-Bridge Inverter

This is a stacked connection of several H-bridge inverters. In this arrangement, the individual H-bridge inverter has the same configuration as a common single-phase, full-bridge inverter. This means that each full-bridge circuit has its own DC source.
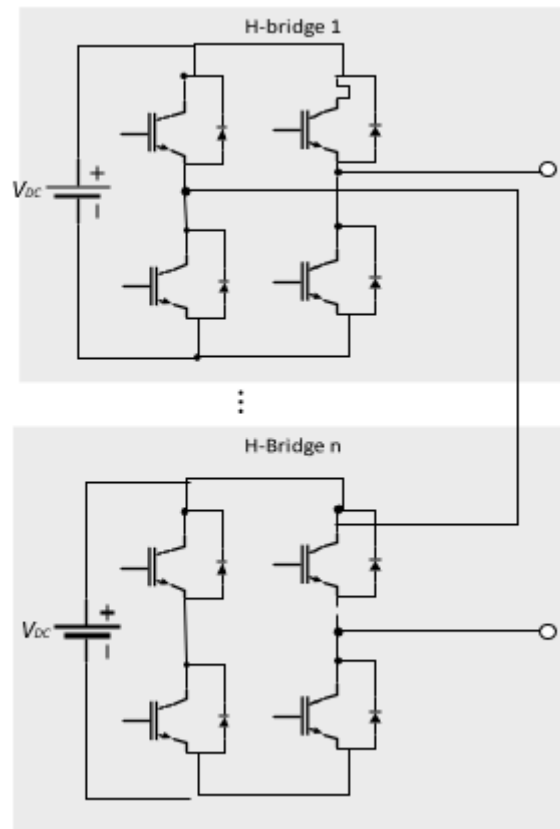
Figure 2.6: Cascaded H-bridge inverter

2.6.3 Flying Capacitor (Capacitor-Clamped) Inverter

The flying capacitor inverter topology eliminates the need to control the dc-link capacitor voltage. Unlike the cascaded topology, it does not require additional voltage sources. Theoretically, this topology can provide an unlimited number of voltage levels; however, practical designs are limited to six voltage levels. This voltage level depends on the number of series-connected power switches.

CHAPTER 3 GRID SYNCHRONIZATION FOR SINGLE-PHASE INVERTERS

3.1 Grid Synchronization

The electric grid is a complex and dynamic system that is impacted by several factors and components, including changes in load, transients, and harmonics. Because of this, it is not adequate to consider the grid variables such as the magnitude of the voltage, the phase angle, and the frequency as constant variables. These grid elements should be constantly and accurately monitored so as to ensure the proper working of the power converters; considering, the bi-directional interaction between the converters and the grid influences the stability, reliability, and safety of the grid.

The importance of monitoring these grid variables is underpinned by several international grid codes in place, which work to regulate solar energy and wind energy systems and their response to steady-state and transient conditions. The international grid codes define the boundaries of the voltage and frequency within which the system should operate to ensure stable operation. Thus, the converters are needed to accurately monitor and take action to regulate the power grid and ensure that the variables do not exceed the set limits. Therefore, it is important to differentiate between two similar terms, grid monitoring and grid synchronization.

Grid monitoring is the process of extracting pertinent information regarding the magnitude, phase angle, and frequency of the grid components. Grid synchronization, on the other hand, involves instantaneously monitoring the electrical grid to ensure that the inverter and the electrical grid are in unison.

For single-phase grid-connected inverters, the accuracy of the synchronization to the grid depends not only on detecting precisely the properties of the grid voltage but also on how the attributes of the voltage can be used to tune the controller to the variations of the power grid. Usually, the properties required for grid synchronization are voltage magnitude and phase angle; however, some techniques have also relied on detecting certain harmonic components and using these for additional functionalities.

Usually, the attributes of the grid detected via grid monitoring are used in controlling the response of the grid to transient. The main attributes of the grid required are the magnitude of the voltage, the phase angle, and the operating frequency. However, other harmonic information can also be extracted for the purpose of ensuring power conditioning and resonance damping. Thus, grid synchronization techniques can be classified into two categories, namely time-domain detection and frequency-domain detection methods.

3.2 Discrete Fourier Transform (DFT)

The Discrete Fourier Transform (DFT) is a digital signal processing technique which is used to estimate the spectral content of a signal. As such, the DFT is useful for identifying harmonic content of the voltage and current of a power system and can be used to compute the fundamental frequency component of certain features of the grid. Literatures [13-15] have adequately reported several applications of the DFT to converter synchronization, including the use of time-varying Fourier coefficients, as well as techniques underpinned by polynomial regression analysis. However, the complexity of DFT computations has led to the rise of a new algorithm referred to as the Fast Fourier Transform (FFT). The FFT offers reduced computation time, but it is not ideal for grid synchronization purposes because the algorithm is not optimal for extracting single-frequency components.

3.3 Phase-Locked Loop

A phase locked loop (PLL) is a closed-loop system that is widely used to monitor and synchronize the power grid. The main component in this system is the internal oscillator which constantly keeps track of the time of a periodic signal via a feedback loop. In this case, the internal oscillator is locked to the grid variables and the amplitude and phase content generated is used by the control system.

The structure describing the operation of the PLL is presented in Figure 3.1, and it is made up of three fundamental blocks,

- The phase detector (PD)

- The loop filter (LF)

- The voltage-controlled oscillator (VCO)
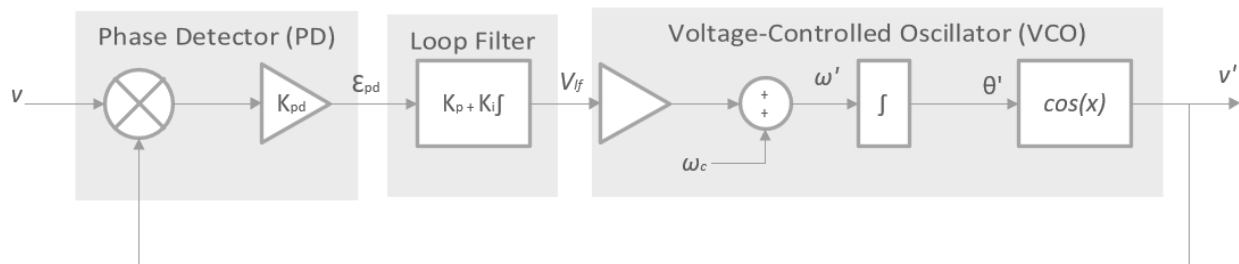
Figure 3.1: Block diagram of a PLL

3.3.1 The Phase Detector (PD)

The output of the internal oscillator in the PLL is fed back to PD and this serves as the reference. The PD also receives the input signal (the voltage from the grid) to generate an output signal. The output signal generated depends on the phase difference between the oscillator-generated signal and the input signal.

3.3.2 The Loop Filter (LF)

A filter is required in most cases where the output of the phase detector contains high-frequency AC components. In general, a low-pass filter is utilized for this purpose. However, a PI controller can also achieve the same function.

3.3.3 The Voltage-Controlled Oscillator (VCO)

The LF provides an input signal to the VCO, and an output AC signal with a shifted frequency is generated.

3.4 Zero-Crossing Detection Method

The zero-crossing detection (ZCD) method is a fundamental method based on the periodic nature of the signal. Figure 3.2 shows how this method works. The point where the signal crosses the zero point is detected after every half period. Because of this, this method is only suitable for stable signals because the result is highly affected by transient and noise.

To compute the angle, a PI controller obtains the angle difference between the desired angle and the angle obtained. The zero-crossing point is then detected by multiplying the current sampled value of the voltage and the previous period. If this value is zero, the phase angle is zero but if it exceeds zero, the angle is π.
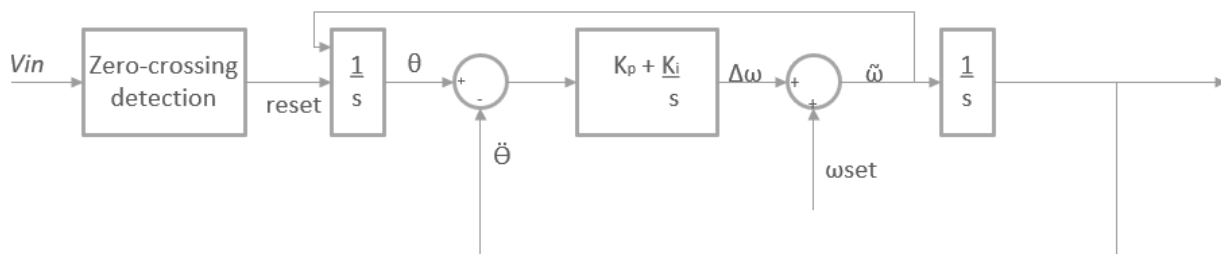
Figure 3.2: Block diagram of the zero-crossing detection method

3.5 Fourier Series

The idea of representing periodic functions by an infinite sum of sinusoidal and/or cosine functions was first proposed by Jean Baptiste Joseph Fourier. In 1807, Fourier proposed a new analysis technique for the solution of differential equations that demonstrated heat flow in a metal plate [16]. This technique makes it possible to determine the frequency components of periodic signals by multiplying the signal by a set of trigonometric functions.

In essence, Fourier posited that every periodic function contained trigonometric components with frequencies that comprise integer multiples of the fundamental frequency of the periodic function. Mathematically, Fourier demonstrated that any periodic function *f(t)* is described as shown

$$f(t) = a_0 + \sum_{n=1}^{\infty} a_n \cos(n\omega t) + b_n \sin(n\omega t) \tag{3.1}$$

where, a_0, a_n, and b_n are known as the Fourier coefficients. The term ω is the fundamental angular frequency of the periodic function and $n\omega$ represents the harmonic frequencies of the function *f(t)*.

3.5.1 Fourier Coefficients

The Fourier coefficients defined in Eqn. 3.1 can be determined using the following expressions

$$a_0 = \frac{1}{T} \int_0^T f(t)dt \tag{3.2}$$

$$a_n = \frac{2}{T} \int_0^T f(t)\cos(n\omega t)dt \tag{3.3}$$

$$b_n = \frac{2}{T} \int_0^T f(t)sin(n\omega t)dt \qquad (3.4)$$

From (3.5), a selective band-pass filter as shown in Figure 3.3 is designed by multiplying the input voltage by respective sine and cosine functions with the fundamental frequency. From the designed filter, it is possible to extract an output that is dependent on the order of the harmonic n. The magnitude and the phase angle of this output is expressed thus

$$V_n = \sqrt{a_n^2 + b_n^2} \qquad (3.5)$$

$$\theta_n = tan^{-1}\frac{a_n}{b_n} \qquad (3.6)$$
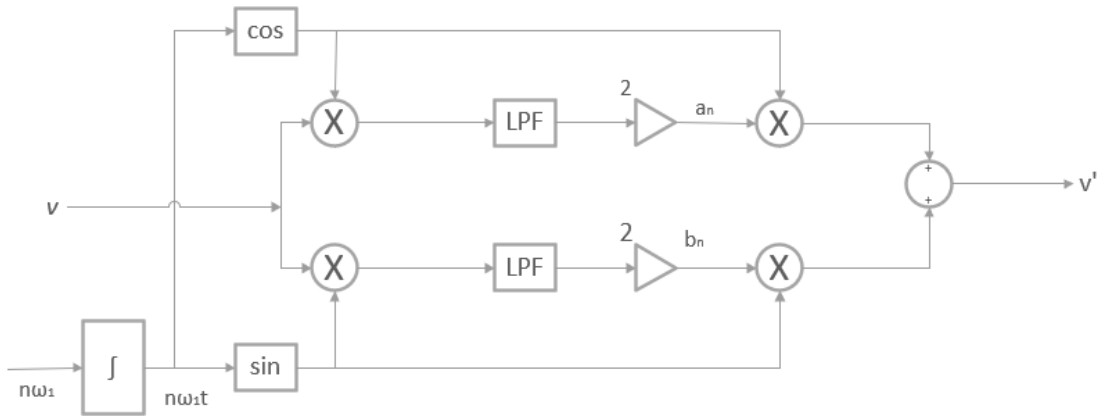
Figure 3.3: Block diagram of the Fourier-series method for grid synchronization

The mean value of the output is extracted using a low pass filter whose cut-off frequency is a function of the lowest frequency component in the signal. Ideally, in a power grid, the lowest frequency component is the fundamental frequency component, which is 50Hz in the United Kingdom, Asia, Africa, and 60Hz in the United States.

CHAPTER 4: PULSE WIDTH MODULATION AND DIRECT POWER CONTROL

This chapter explores the different modulation methods for a single-phase inverter. Common techniques such as sinusoidal pulse width modulation (SPWM), third harmonic injection pulse width modulation, and space vector pulse width modulation are explained. Subsequently, control structures for grid-connected systems are studied, and the direct power control technique used in this thesis is presented.

4.1 Sinusoidal Pulse Width Modulation

The sinusoidal pulse width modulation (SPWM) compares a low-frequency sinusoidal wave (which is often the reference) to a carrier wave (usually a triangular wave or a sawtooth wave) to generate switching signals for the inverter. If a triangular wave is used, then it is referred to as a double-edge naturally sampled modulation. This is because both the rising and the falling edges of the signal account for the modulation. For a sawtooth wave, the modulation is named trailing edge naturally sampled modulation because only the trailing edge is taken into consideration. The switching signals square pulses which repeat after every half cycle, and the square pulse can be adjusted accordingly to increase or decrease the output. The frequency of the complimentary wave is the switching frequency of the inverter, and the fundamental frequency of the generated waves is the frequency of the sine wave.

The reference sine wave is defined by the following equation

$$v_{sin} = Mcos(w_0t + \theta_0) \tag{4.1}$$

where,

M is modulation index, usually between 0 and 1,

w_0 is desired output frequency, and

θ_0 is phase angle.

4.2 Third-Harmonic Injection Pulse Width Modulation

SPWM is a modulation scheme that is easy to implement, and it is the most commonly used method. However, this technique does not completely use the available DC bus supply voltage, and the implication of this is the reduction in the maximum output voltage available. The research carried out by Mohan et al. [17] showed that upon the rectification of a three-phase input voltage, the output voltage is the line-to-line voltage boosted by 135%. It is possible to boost the output voltage by adding the third harmonic component of the fundamental frequency to the sinusoidal signal. The third harmonic components cancel out because the phase shift of the third harmonic component is 3 x 120 = 360^0, leading to a sinusoidal output voltage.

4.3 Space Vector Pulse Width Modulation

The space-vector pulse width modulation is a preferred modulation schemes used today. It has increased in popularity as a result of the optimal utilization of bus voltage offered, as well as the reduction in commutation losses.

SVPWM algorithm for three-level single-phase inverters is being used in this paper. To generate appropriate switching signals, this algorithm needs several inputs, including DC voltage for MPPT control, the voltages of the balance capacitors, AC output current, sampling time, and the outputs. In the SVPWM technique, the reference vector is generated by a control strategy and is the product of the combination of other possible state vectors.

In order to determine the region of operation, the phase voltage for every possible combination of the switches is computed. In the case of a three-level, single-phase inverter, we

can have three distinct output levels. The possible state vectors are represented in Table 4.1. The state is classified as -1 for the lowest possible output phase voltage and 1 for the maximum output phase voltage possible. The calculation of the output voltage

The single-phase three-level inverter topology consists of two legs (A and B), and on each leg, there are four bi-directional switches and two clamping diodes.

The switching states of the inverter are defined in Table 4.1.

Table 4.1: Switching states and output for SVPWM

Switching State	S_{A1}	S_{A2}	S_{A3}	S_{A4}	S_{B1}	S_{B2}	S_{B3}	S_{B4}
1(P)	ON	ON	OFF	OFF	ON	ON	OFF	OFF
0(O)	OFF	ON	ON	OFF	OFF	ON	ON	OFF
-1(N)	OFF	OFF	ON	ON	OFF	OFF	ON	ON

In table 4.2, the value of the reference voltage at different states is calculated. The grid voltage, V_{ab} is synthesized periodically and this voltage is calculated as a linear combination of the space vectors (a function of the capacitor voltage), and this is used as the input of the modulator.

$$V_{ref} = \sqrt{V_d{}^2 + V_q{}^2} \tag{4.1}$$

$$\delta = tan^{-1}\frac{V_d}{V_q} \tag{4.2}$$

$$\varphi = \omega_0 t - \delta - \frac{\pi}{2} \tag{4.3}$$

Table 4.2: Value of reference voltage at different switching states

STATE	S_a	S_b	V_a	V_b	V_{ab}
1	1	1	$E/2$	$E/2$	0
2	1	0	$E/2$	0	$E/2$
3	1	-1	$E/2$	$-E/2$	E
4	0	1	0	$E/2$	$-E/2$
5	0	0	0	0	0
6	0	-1	0	$-E/2$	$E/2$
7	-1	1	$-E/2$	$E/2$	$-E$
8	-1	0	$-E/2$	0	$-E/2$
9	-1	-1	$-E/2$	$-E/2$	0

Considering the different switching combinations in a three-level inverter, there are nine states of operation that the power switches can potentially assume. These states can be classified into the following groups;

- Zero voltage vector group (PP, OO, NN)

- Small voltage vector group (PO, ON, NO, OP), and

- Large voltage vector group (PN, NP),

With this classification, we have of four (4) regions of operation as shown in Figure 4.1.
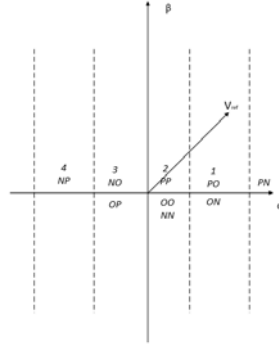
Figure 4.1: Region of operation of each voltage vector

The zero-voltage vector has 3 switching states that are redundant while the small voltage vector has 2 redundant switching states. This redundancy is effective for balancing the charge in each DC-link capacitor.

4.3.1 Dwelling Time Calculation

According to the volt-seconds principle, the time interval of each voltage vector can be calculated

$$V_{ab}T_s = V_1T_1 + V_2T_2 \tag{4.4}$$

The real component of the voltage vector V_α, and the value of the DC-link capacitor E are used to calculate the time at which each output voltage vector is in operation.

Table 4.3: Calculation of dwelling time

Region/time	T_1	T_2
1	$2(E - V_\alpha)T_s/E$	$(2V_\alpha - E)T_s/E$
2	$2V_\alpha T_s/E$	$(E - 2V_\alpha)T_s/E$
3	$-2V_\alpha T_s/E$	$(E + 2V_\alpha)T_s/E$
4	$2(E + V_\alpha)T_s/E$	$-(2V_\alpha + E)T_s/E$

4.3.2 Modifying the Sequence of Switching

There's a lot of emphasis placed on minimizing losses due to switching, as well as avoid a sudden huge jump in the voltage vectors selected, it is important to leverage a switching algorithm which makes use of 5 modulation vectors from every vector group. The switching sequence is selected such that the small vectors are used first and last. Table 4.4 shows the output voltage vector for each region.

Table 4.4: Switching sequence for SVPWM

Region	Switching Sequence
1	PO-PN-ON-PN-PO
2	PO-OO-ON-OO-PO
3	OP-OO-NO-OO-OP
4	OP-NP-NO-NP-OP

4.3.3 Neutral-Point Balancing

Under ideal conditions, it is expected that the voltage across the DC-link capacitors are equally divided but, this is not the case in normal operating conditions. Without an optimal strategy for controlling this interaction, the harmonic content of the voltage will exceed the threshold, and this will inadvertently shorten the lifespan of the switching devices. A neutral-point control strategy is adopted to modify the operating time for vectors that are redundant.

Hence, a voltage-adjusting coefficient (*f)* is proposed to modify the effective time of the voltage vectors. The adjustment is based on the direction of the load current, as well as the capacitor voltage. New operating times, $T_p,$ and T_n are proposed, and the values are controlled by the flow of the current and the voltage error.

$$T_p = fT_0 \qquad (4.5)$$

$$T_n = (1 - f)T_0 \qquad (4.6)$$

4.4 Control Structures for Grid-Connected Systems

Another crucial aspect of an inverter is the control structure, which determines the power flow management, as well as the modulation. The different structures commonly adopted are explored, and the method used in this thesis is ultimately presented.

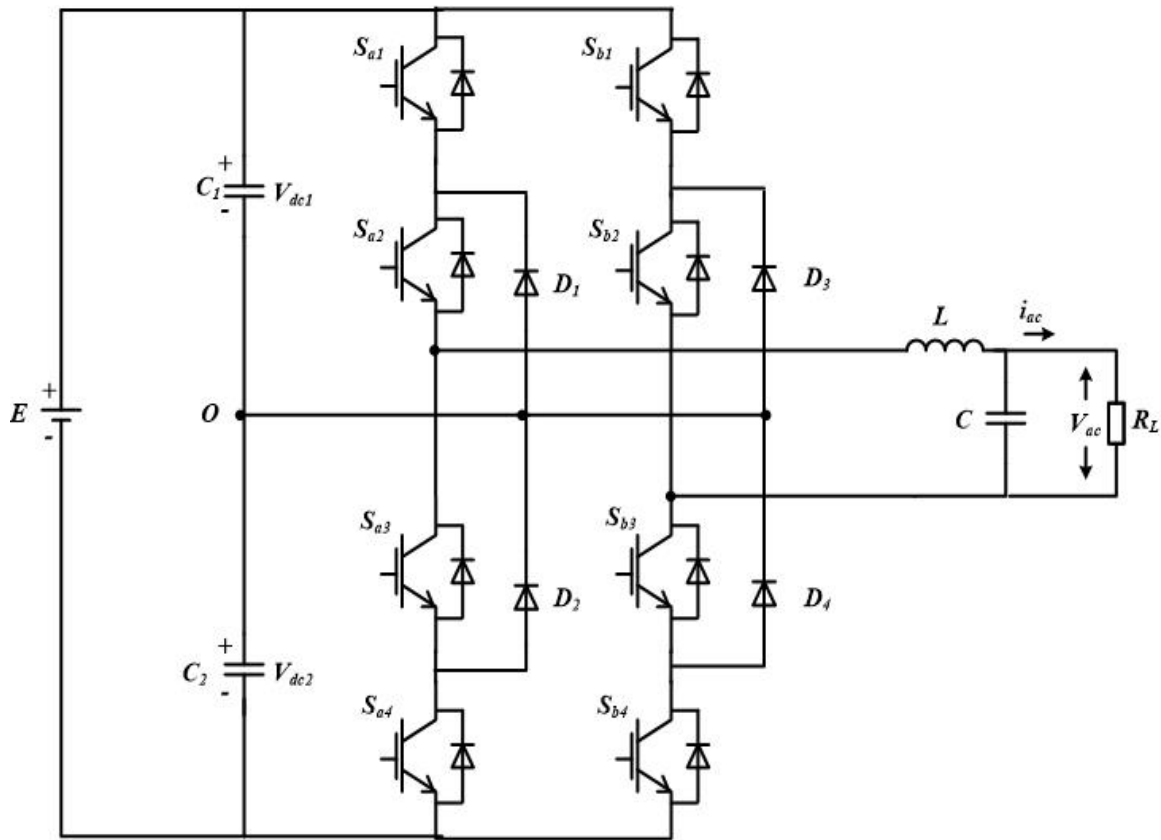### 4.4.1 Stationary Reference Frame Control

Figure 4.2: Single-phase three-level neutral point clamped inverter

In a stationary reference frame controller, the current from the grid is converted to the stationary reference frame α-β. Using Figure 4.1, the mathematical expression of the circuit is as follows,

$$L\frac{dI_L}{dt} + r_L I_L = V - V_{grid} \tag{4.6}$$

$$I_L = C\frac{dv_c}{dt} + \frac{V_{grid}}{Z} \tag{4.7}$$

The grid current is then transformed into the time-varying quantities as

$$I_\alpha = C\frac{dv_{\alpha c}}{dt} + \frac{V_\alpha}{Z} \tag{4.8}$$

$$I_\beta = C\frac{dv_{\beta c}}{dt} + \frac{V_\beta}{Z} \tag{4.9}$$

where,

V_α is the real output voltage,

V_β is the imaginary output voltage,

I_α is the real inductor current,

u_α is the real inverter average sinusoidal duty ratio,

I_β is the imaginary inductor current, and

u_β is the imaginary inverter average sinusoidal duty ratio.

Substituting the value of (4.8) and (4.9) into (4.6), we have,

$$L\frac{dI_\alpha}{dt} + r_L I_\alpha = u_\alpha - V_\alpha \tag{4.10}$$

45

$$L\frac{dI_\beta}{dt} + r_L I_\beta = u_\beta - V_\beta \tag{4.11}$$

$$I_\alpha = C\frac{dv_{\alpha c}}{dt} + \frac{V_\alpha}{z} \tag{4.12}$$

$$I_\beta = C\frac{dv_{\beta c}}{dt} + \frac{V_\beta}{z} \tag{4.13}$$

$$V_\alpha = v_{\alpha c} + C\frac{dv_{\alpha c}}{dt}r_c \tag{4.14}$$

$$V_\beta = v_{\beta c} + C\frac{dv_{\beta c}}{dt}r_c \tag{4.15}$$

Expanding (4.6), we have,

$$L\frac{dI_\alpha}{dt} + r_L I_\alpha = u_\alpha - \left[v_{\alpha c} + C\frac{dv_{\alpha c}}{dt}r_c\right] \tag{4.16}$$

$$L\frac{dI_\beta}{dt} + r_L I_\beta = u_\beta - \left[v_{\beta c} + C\frac{dv_{\beta c}}{dt}r_c\right] \tag{4.17}$$

$$I_\alpha = C\frac{dv_{\alpha c}}{dt} + \frac{1}{z}\left[v_{\alpha c} + C\frac{dv_{\alpha c}}{dt}r_c\right] \tag{4.18}$$

$$I_\beta = C\frac{dv_{\beta c}}{dt} + \frac{1}{2}\left[v_{\beta c} + C\frac{dv_{\beta c}}{dt}r_c\right] \tag{4.19}$$

4.4.2 Synchronous Reference Frame Control

From the stationary reference frame equations, it is possible to obtain the *d-q* model of the inverter. This *d-q* model can be achieved by using the transformation matrix in (4.20).

$$\begin{bmatrix} X_d \\ X_q \end{bmatrix} = T\begin{bmatrix} X_\alpha \\ X_\beta \end{bmatrix} \tag{4.20}$$

$$\begin{bmatrix} X_\alpha \\ X_\beta \end{bmatrix} = T^{-1} \begin{bmatrix} X_d \\ X_q \end{bmatrix} \tag{4.21}$$

$$T = \begin{bmatrix} cos\omega t & sin\omega t \\ -sin\omega t & cos\omega t \end{bmatrix} \tag{4.22}$$

$$T^{-1} = \begin{bmatrix} cos\omega t & -sin\omega t \\ sin\omega t & cos\omega t \end{bmatrix} \tag{4.23}$$

In order to separate the *d-q* components, the resistive components are neglected because the values are relatively small. Also, the chain rule is applied to the transformation matrix and the resultant average state-space equation is as follows.

$$\frac{d}{dt} \begin{bmatrix} I_d \\ I_q \end{bmatrix} = \frac{1}{L} \begin{bmatrix} u_d \\ u_q \end{bmatrix} + \begin{bmatrix} 0 & -\omega \\ \omega & 0 \end{bmatrix} \begin{bmatrix} I_d \\ I_q \end{bmatrix} - \frac{1}{L} \begin{bmatrix} V_d \\ V_q \end{bmatrix} \tag{4.24}$$

$$\frac{d}{dt} \begin{bmatrix} V_d \\ V_q \end{bmatrix} = \frac{1}{C} \begin{bmatrix} I_d \\ I_q \end{bmatrix} + \begin{bmatrix} 0 & -\omega \\ \omega & 0 \end{bmatrix} \begin{bmatrix} V_d \\ V_q \end{bmatrix} - \frac{1}{CZ} \begin{bmatrix} V_d \\ V_q \end{bmatrix} \tag{4.25}$$

The *d-q* model of the inverter is then computed as

$$L\frac{di_d}{dt} = v_d - Ri_d + \omega Li_q - v_{abd} \tag{4.26a}$$

$$L\frac{di_q}{dt} = v_q - Ri_q - \omega Li_d - v_{abq} \tag{4.26b}$$

4.5 Single-Phase Inverter Model

In a bid to express the voltage component of the inverter in terms of the harmonics and the DC component, we have the following equation

$$v = v_m sin(\omega t) + \sum_{n=2}^{\infty} v_n sin(n\omega t + \varphi_{un}) + v_{DC} \tag{4.27}$$

$$v = v_m sin(\omega t) + v_H \tag{4.28}$$

$$i = i_m \sin(\omega t + \varphi) + \sum_{n=2}^{\infty} i_n \sin(n\omega t + \varphi_{un}) + i_{DC} \qquad (4.29)$$

$$i = i_d \sin(\omega t) + i_q \cos(\omega t) + i_H \qquad (4.30)$$

$$v_{ab} = v_{abm} \sin(\omega t + \varphi_{ab}) \qquad (4.31)$$

And both the grid voltage and grid current are considered to consist of both their fundamental component and their harmonic component. According to the definition in (1), the current and voltage can be expressed in the d-q synchronous rotating frame as

$$i_d = i_m \cos(\varphi), i_q = i_m \sin(\varphi) \qquad (4.32)$$

$$v_{abd} = v_{abm} \cos(\varphi_{ab}), v_{abq} = v_{abm} \sin(\varphi_{ab}) \qquad (4.33)$$

By substituting (4.26) in (4.32) and (4.33), we have the *d-q* component of the voltages as

$$v_{abd} = v_m - Ri_d - L\frac{di_d}{dt} + \omega Li_q \qquad (4.34)$$

$$v_{abq} = -Ri_q - L\frac{di_q}{dt} - \omega Li_d \qquad (4.35)$$

4.6 Direct Power Control
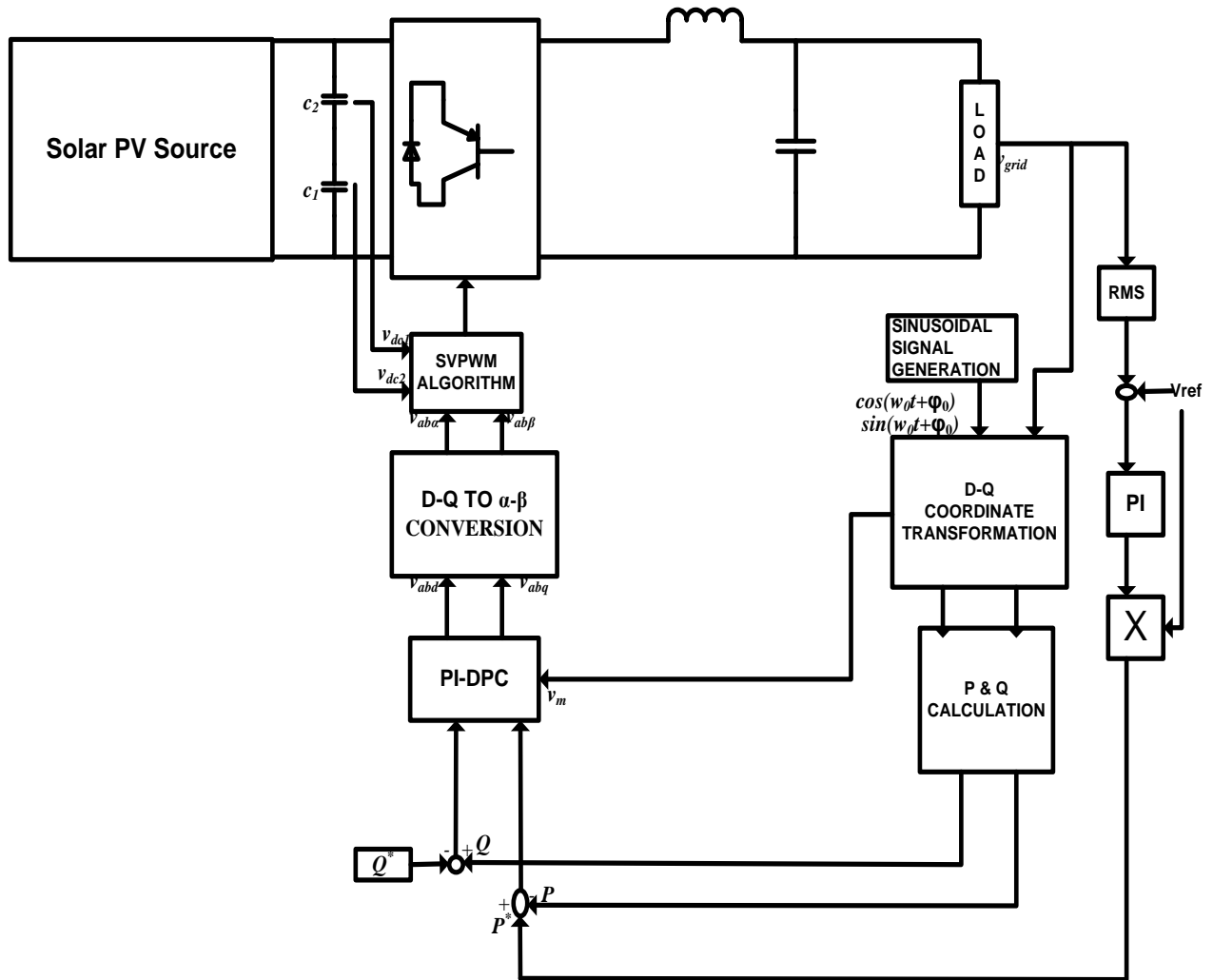
Figure 4. 3: Direct power control for single-phase inverters

The basic structure of the direct power control (DPC) scheme is as shown in Figure 4.2. The DPC eliminates the use of an internal current control loop and a pulse width modulation block. With DPC, a switching table controls the selection of the switching states of the converter. This table is computed using the error between the actual values and the desired values of the real & reactive power. Because of this, it is then important that the estimation of these values is done accurately and swiftly.

According to instantaneous power theory, the active power P and the reactive power Q can be expressed as

$$\begin{bmatrix} P \\ Q \end{bmatrix} = \frac{1}{2}\begin{bmatrix} v_d & v_q \\ v_q & -v_d \end{bmatrix}\begin{bmatrix} i_d \\ i_q \end{bmatrix} = \frac{1}{2}\begin{bmatrix} v_\alpha & v_\beta \\ v_\beta & -v_\alpha \end{bmatrix}\begin{bmatrix} i_\alpha \\ i_\beta \end{bmatrix} \tag{4.36}$$

As described previously, v_α, v_β, i_α and i_β, are the α-β components of the main voltage and the current respectively. From (4.36), we can compute the differential values of the P and Q. This is expressed as

$$\begin{bmatrix} \dfrac{dP}{dt} \\ \dfrac{dQ}{dt} \end{bmatrix} = \frac{1}{2}\begin{bmatrix} v_d & v_q \\ v_q & -v_d \end{bmatrix}\begin{bmatrix} \dfrac{di_d}{dt} \\ \dfrac{di_q}{dt} \end{bmatrix} \tag{4.37}$$

Substituting these components into (4.26), we have

$$\begin{bmatrix} v_{abd} \\ v_{abq} \end{bmatrix} = \begin{bmatrix} v_d \\ v_q \end{bmatrix} - \frac{2L}{v_d{}^2 + v_q{}^2}\begin{bmatrix} v_d\dfrac{dP}{dt} & v_q\dfrac{dQ}{dt} \\ v_q\dfrac{dP}{dt} & -v_d\dfrac{dQ}{dt} \end{bmatrix}$$
$$- \frac{2}{v_d{}^2 + v_q{}^2}\begin{bmatrix} (Rv_d - \omega Lv_q) & (Ru_q + \omega Lv_d) \\ (Rv_q + \omega Lv_d) & -(Ru_d - \omega Lv_q) \end{bmatrix}\begin{bmatrix} P \\ Q \end{bmatrix}$$

$$\tag{4.38}$$

Taking the voltage vector to be oriented to the d-axis, we have the components further simplified to be

$$\begin{bmatrix} v_{abd} \\ v_{abq} \end{bmatrix} = \begin{bmatrix} v_m \\ 0 \end{bmatrix} - \frac{2L}{v_m}\begin{bmatrix} \dfrac{dP}{dt} \\ -\dfrac{dQ}{dt} \end{bmatrix} - \frac{2}{v_m}\begin{bmatrix} RP + \omega LQ \\ -RQ + \omega LP \end{bmatrix} \tag{4.39}$$

where V_m is the grid voltage.

Splitting the d-q components gives us

$$\begin{cases} v_{abd} = -\dfrac{2L}{v_m}\dfrac{dP}{dt} + v_m - \dfrac{2RP}{v_m} - \dfrac{2\omega LQ}{v_m} \\ v_{abq} = \dfrac{2L}{v_m}\dfrac{dQ}{dt} + \dfrac{2RQ}{v_m} - \dfrac{2\omega LP}{v_m} \end{cases} \tag{4.40}$$

Equation (4.40) contains both steady-state and dynamic components. However, it is advantageous if the dynamic components are replaced by PI controllers. This is shown in (4.41).

$$\begin{cases} v_{abd} = -\left[K_{Pp} + \dfrac{K_{Pi}}{s}\right](P^* - P) + v_{ds} \\ v_{abq} = \left[K_{Qp} + \dfrac{K_{Qi}}{s}\right](Q^* - Q) + v_{qs} \end{cases} \tag{4.41}$$

In (4.41), the reference value P^* is estimated via the DC-link voltage. The reactive power reference Q^* is set to 0 in a bid to ensure that the power factor is 1.

Based on the transformation matrix derived earlier, we calculate the alpha-beta components of the voltage using the fundamental components

$$\begin{bmatrix} v_{ab\alpha} \\ v_{ab\beta} \end{bmatrix} = \begin{bmatrix} \cos \omega_0 t & \sin \omega_0 t \\ \sin \omega_0 t & -\cos \omega_0 t \end{bmatrix} \begin{bmatrix} v_{abd} \\ v_{abq} \end{bmatrix} \tag{4.42}$$

4.6.1 Novel Power Calculation Strategy

The methodology proposed in this paper first requires the generation of sinusoidal signals whose angular frequency ω_0 and phase angle φ_0 are the nominal angular frequency and initial angle of the grid voltage respectively. The generated sinusoidal signals are then multiplied by the grid voltage. This multiplication causes the components to be split into the sin and cosine components shown in (4.43).

$$v_{sin} = v\sin(\omega_0 t + \varphi_0) = [v_m \sin \omega t + v_H]\sin(\omega_0 t + \varphi_0) \tag{4.43}$$

$$v_{sin} = v_{sinH} + v_{sinL} \tag{4.44}$$

$$v_{cos} = v\cos(\omega_0 t + \varphi_0) = [v_m \sin\omega t + v_H]\cos(\omega_0 t + \varphi_0) \tag{4.45}$$

$$v_{cos} = v_{cosH} + v_{cosL} \tag{4.46}$$

Usually, if a PLL was employed to compute the angular frequency of the grid voltage, β as is zero, making the low-frequency components DC components. However, in this case, a PLL is not used, and the orthogonal low-frequency components can be extracted using a low pass filter. The output of this filter gives

$$\begin{cases} v_{LPq} = v_{cosL} = v_m \dfrac{1}{2}\sin(\beta - \varphi_0) \\[2mm] v_{LPd} = v_{sinL} = v_m \dfrac{1}{2}\cos(\beta - \varphi_0) \\[2mm] i_{LPq} = i_{cosL} = i_m \dfrac{1}{2}\sin(\beta + \varphi - \varphi_0) \\[2mm] i_{LPd} = i_{sinL} = i_m \dfrac{1}{2}\cos(\beta + \varphi - \varphi_0) \end{cases} \tag{4.47}$$

The harmonics present in the grid current and voltage components are usually much smaller in comparison with the fundamental value of the respective component. Because of this, the angular frequency of the components i_{sinH}, i_{cosH}, v_{sinH}, and v_{cosH}, are considered to be approximately $\omega_0 + \omega$. In this case, a notch filter (NF) with a frequency which is twice the fundamental frequency is used to obtain the components. The low-frequency components, i_{sinL}, and i_{cosL} are obtained using a low pass filter (LPF). The LPF extracts the low-frequency components of the voltage. The use of an LPF ensures that the higher-order harmonics are eliminated.

As a result of the d-q components being orthogonal to one another, the grid voltage can be expressed thus

$$v_m = 2\sqrt{v_{LFd}^2 + v_{LFq}^2} \tag{4.48}$$

From (4.36), active and reactive power is expressed as

$$\begin{cases} P = \dfrac{1}{2} v_m i_m \cos(\varphi) \\ Q = -\dfrac{1}{2} v_m i_m \sin(\varphi) \end{cases} \tag{4.49}$$

Substituting the values of (4.47) in (4.49), we have

$$\begin{cases} P = 2(v_{LFd} i_{LFd} + v_{LFq} i_{LFq}) \\ Q = 2(v_{LFq} i_{LFd} - v_{LFd} i_{LFq}) \end{cases} \tag{4.50}$$

4.6.2 Group Delay

When signals pass through a signal, the frequency components of the signals are delayed. This delay is defined as the group delay and is described thus

$$\tau_d(\omega) = -\frac{\partial \theta(\omega)}{\partial \omega} \tag{4.51}$$

In ideal filters, the phase is linear, and so this translates to a constant delay. However, in practical situations (and for the case of this thesis), there are variations in the phase. This means there is a phase delay, and this causes the low-frequency components derived in (4.47) to not satisfy the conditions.

$$\begin{cases} v_{LPq} \neq v_{cosL} = v_m \dfrac{1}{2} \sin(\beta - \varphi_0) \\ v_{LPd} \neq v_{sinL} = v_m \dfrac{1}{2} \cos(\beta - \varphi_0) \\ i_{LPq} \neq i_{cosL} = i_m \dfrac{1}{2} \sin(\beta + \varphi - \varphi_0) \\ i_{LPd} \neq i_{sinL} = i_m \dfrac{1}{2} \cos(\beta + \varphi - \varphi_0) \end{cases} \tag{4.52}$$

4.6.3 Filter Design

Based on the group delay characteristics, a Butterworth filter is designed. This filter is a second-order filter, and the transfer function of both LPF and NF are

$$G_{LPF}(s) = \frac{\omega_{fL}^2}{s^2 + \mu\omega_{fL}s + \omega_{fL}^2} \tag{4.53}$$

$$G_{NF}(s) = \frac{s^2 + \omega_{fL}^2}{s^2 + \mu\omega_{fN}s + \omega_{fN}^2} \tag{4.54}$$

where,

μ is the quality factor (chosen as 0.707)

ω_{fL} is the cut-off frequency of the low-pass filter, and

ω_{fN} is the center frequency of the notch filter

The group delay of both filters can be calculated thus

$$\theta_{LPF}(\omega) = \text{-}\pi + \tan^{-1}\left(\frac{\mu}{\omega/\omega_{fL} - \omega_{fL}/\omega}\right) \tag{4.55}$$

$$\theta_{LPF}(\omega) = tan^{-1}\left(\frac{\mu}{\omega/\omega_{fL} - \omega_{fL}/\omega}\right) \tag{4.56}$$

$$\theta_{NF}(\omega) = -\pi + tan^{-1}\left(\frac{\mu}{\omega/\omega_{fN} - \omega_{fN}/\omega}\right) \tag{4.57}$$

The first equation is valid when $\omega \geq \omega_{fL}$, and the second equation applies when $\omega < \omega_{fL}$.

Usually, the angular frequency of low-frequency components is negligible in comparison with the angular frequency of notch filter components (ω_{fN}), θ_{NF} tends to 0. However, θ_{LPF} is considered in this paper because the main voltage distortion is minimized by setting the cutoff frequency of the low pass filter to be small. We also introduce a new component, φ_e which is the phase error resulting from the LPF. The low-frequency components in (4.52) are now expressed as

$$
\begin{cases}
v_{LPd} = \dfrac{1}{2} v_{grid} cos(\beta - \varphi_0 - \varphi_e) \\
v_{LPq} = \dfrac{1}{2} v_{grid} sin(\beta - \varphi_0 - \varphi_e)
\end{cases}
\tag{4.58}
$$

P and Q from (4.50) is then recomputed as

$$
\begin{bmatrix} P \\ -Q \end{bmatrix} = 2 \begin{bmatrix} v_{LFd} & v_{LFq} \\ -v_{LFq} & v_{LFd} \end{bmatrix} \begin{bmatrix} i_{LFd} \\ i_{LFq} \end{bmatrix} = \frac{1}{2} \begin{bmatrix} v_{grid} i_{grid} cos(\varphi - \varphi_e) \\ v_{grid} i_{grid} sin(\varphi - \varphi_e) \end{bmatrix}
\tag{4.59}
$$

This equation shows that the phase error (φ_e) will lead to deterioration of the power calculation technique. Therefore, the low pass filter needs a compensation scheme to improve the precision.

4.6.4 Phase-Compensation and Phase Deviation Calculation

Since the group delay characteristics of the low pass filter will lead to phase delay which reduced the precision of the power components computed, certain compensation factors are required.

First, a frequency compensation matrix is introduced.

$$
C_f = \begin{bmatrix} cos(\beta - \varphi_0 - \varphi_e) & sin(\beta - \varphi_0 - \varphi_e) \\ -sin(\beta - \varphi_0 - \varphi_e) & cos(\beta - \varphi_0 - \varphi_e) \end{bmatrix}
\tag{4.60}
$$

Another sinusoidal matrix is defined in (4.61).

$$C_0 = \begin{bmatrix} sin(\omega_0 t + \varphi_0) & cos(\omega_0 t + \varphi_0) \\ cos(\omega_0 t + \varphi_0) & -sin(\omega_0 t + \varphi_0) \end{bmatrix} \tag{4.61}$$

The sinusoidal components of the grid voltage are then expressed in terms of the compensation matrix as shown in (4.62).

$$\begin{bmatrix} sin(\varphi - \varphi_e) \\ cos(\varphi - \varphi_e) \end{bmatrix} = C_f C_0 \begin{bmatrix} 1 \\ 0 \end{bmatrix} \tag{4.62}$$

Multiplying both sides of (4.62) with the main voltage (similar to (4.43)), the results are as follows

$$\begin{cases} \varphi_{sin} = vsin(\omega t - \varphi_e) = \varphi_{sinH} + \varphi_{sinDC} \\ \varphi_{cos} = vcos(\omega t - \varphi_e) = \varphi_{cosL} + \varphi_{cosDC} \end{cases} \tag{4.63}$$

Where

$$\begin{cases} \varphi_{sinH} = -\dfrac{1}{2}v_{grid}cos(2\omega t - \varphi_e) + v_H sin(\omega t - \varphi_e) \\ \varphi_{sinDC} = \dfrac{1}{2}v_{grid}cos(\varphi_e) \\ \varphi_{cosL} = \dfrac{1}{2}v_{grid}sin(2\omega t - \varphi_e) + v_H cos(\omega t - \varphi_e) \\ \varphi_{cosDC} = \dfrac{1}{2}v_{grid}sin(\varphi_e) \end{cases} \tag{4.64}$$

An LPF is required to obtain the φ_{sinDC} and φ_{cosDC}. In this case, there's no phase delay between the input and the output of the LPF. Figure 4.3 shows this
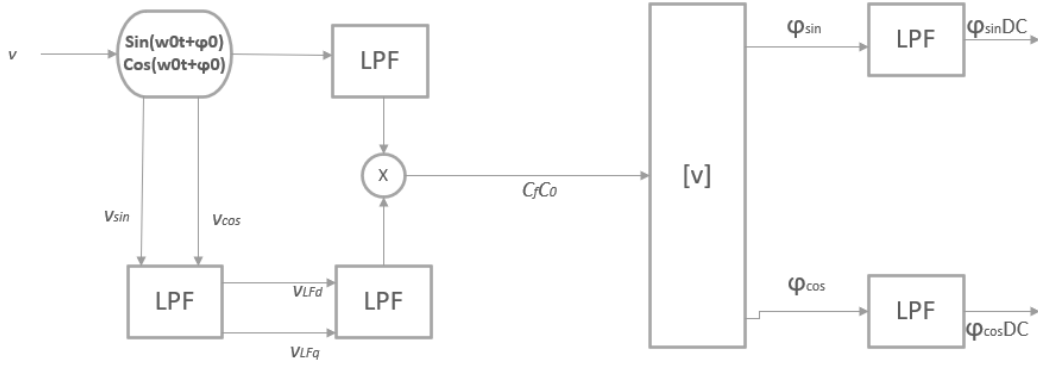
Figure 4.4: Propagation of sine and cosine signals and extraction of DC components

Another compensation matrix, known as the phase deviation matrix, is defined as shown

$$C_\varphi = \begin{bmatrix} cos\varphi_e & -sin\varphi_e \\ sin\varphi_e & cos\varphi_e \end{bmatrix} = \frac{2}{v_{grid}} \begin{bmatrix} \varphi_{sinDC} & \varphi_{cosDC} \\ -\varphi_{cosDC} & \varphi_{sinDC} \end{bmatrix} \tag{4.65}$$

From (4.59), if the RHS is multiplied by C_φ, the active and reactive power components are then expressed as

$$\begin{bmatrix} P \\ -Q \end{bmatrix} = v_{grid} C_\varphi^T C_f \begin{bmatrix} i_{LFd} \\ i_{LFq} \end{bmatrix} = \frac{1}{2} \begin{bmatrix} cos\varphi_e & -sin\varphi_e \\ sin\varphi_e & cos\varphi_e \end{bmatrix} \begin{bmatrix} v_{grid} i_{grid} \cos(\varphi - \varphi_e) \\ v_{grid} i_{grid} \sin(\varphi - \varphi_e) \end{bmatrix}$$
$$= \frac{1}{2} \begin{bmatrix} v_m i_m \cos(\varphi) \\ v_m i_m \sin(\varphi) \end{bmatrix}$$

$$\tag{4.66}$$

where, C_φ^T is the transpose of C_φ.

If both sides of (4.62) are further multiplied by C_φ, we can represent the sinusoidal signals in terms of the compensation matrix as follows

$$C_\varphi \begin{bmatrix} sin(\omega t - \varphi_e) \\ cos(\omega t - \varphi_e) \end{bmatrix} = \begin{bmatrix} cos\varphi_e & sin\varphi_e \\ -sin\varphi_e & cos\varphi_e \end{bmatrix} \begin{bmatrix} sin(\omega t - \varphi_e) \\ cos(\omega t - \varphi_e) \end{bmatrix} \tag{4.67}$$

The sinusoidal signals are then expressed as

57

$$\begin{bmatrix} sin(\omega t) \\ cos(\omega t) \end{bmatrix} = C_\varphi C_f C_0 \begin{bmatrix} 1 \\ 0 \end{bmatrix} \tag{4.68}$$

With the derived compensation matrix, the co-ordinate transformation α-β to *d-q* matrix in (4.23) is then expressed thus

$$\begin{bmatrix} v_{ab\alpha} \\ v_{ab\beta} \end{bmatrix} = C_\varphi C_f C_0 \begin{bmatrix} v_{abd} \\ v_{abq} \end{bmatrix} \tag{4.69}$$
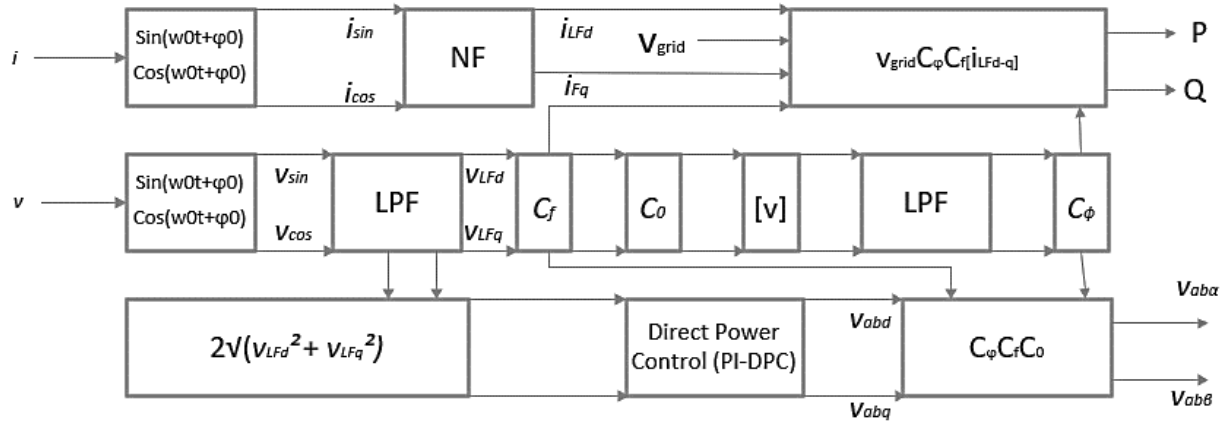

Figure 4.5: Overview of novel control and compensation strategy

CHAPTER 5: SIMULATION RESULTS AND DISCUSSION

5.1 Chapter Overview

The previous three chapters have adequately introduced the theory supporting the research work presented in this thesis. The underlying technology for the direct power control of the three-level, single-phase inverter is demonstrated using MATLAB/Simulink. In this chapter, we carry out an analysis of the results obtained to justify the performance of the methodology presented in this thesis. The quality of the PV system is usually determined by the quality of the voltage, frequency, harmonics, and power factor. Failure to attain the highest standards may require disconnection of the photovoltaic system from the utility. Hence, the effectiveness of the strategy presented is judged according to these factors.

The design of the grid-connected solar PV system is based on the following parameters.

Table 5.1: Design parameters for MATLAB/Simulink simulation

Parameter	Value
Temperature (˚C)	25
Load (Ω)	40-25
Switching frequency (kHz)	1.5
DC-link capacitor (uF)	3300
Grid-side inductor (mH)	10
Grid-side Capacitor (µF)	1000
Quality factor (µ) of low-pass filter and notch filter	0.707
Cut-off frequency of low-pass filter (Hz)	5
Stop-band frequency of notch filter (Hz)	100

5.2 Simulation and Analysis

The modeling of the system is executed in MATLAB/Simulink and a Trina Solar array is taken from the National Renewable Energy Laboratory archive in MATLAB. This array consists of 4-module string and 1 parallel string and this gives us a multiplied voltage output as desired. The control scheme is implemented on an NPC converter and the neutral point capacitor is modeled to ensure that charge balancing is achieved. The control algorithm for the switching of the inverter legs is modeled and fed into the SVPWM pulse port. A filter is also designed to give a desired output sinusoidal waveform.
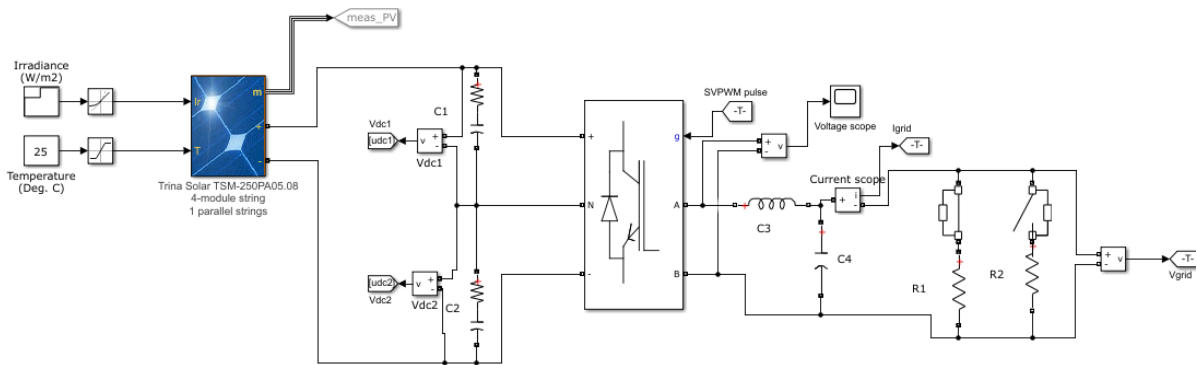

Figure 5.1: Simulation of Single-phase PV system in MATLAB/Simulink

5.2.1 Simulation of Solar PV Array

The PV Array block in MATLAB/Simulink is based on preset modules taken from the archive of the National Renewable Energy Laboratory (NREL).

The irradiance of the solar PV module is set to [250, 750, 1000, 750] at the time [0, 0.2, 1.5, 3]. The output of the solar PV is as shown. The graph shows that the voltage and output power closely track the reference.
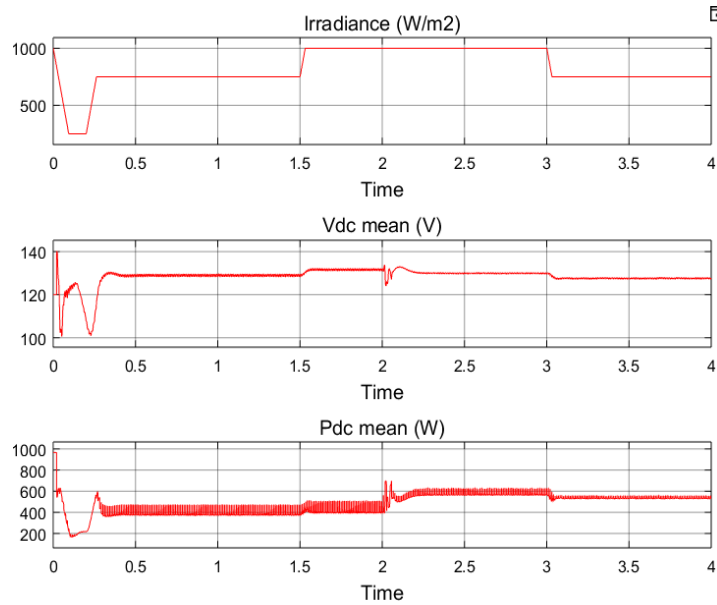
Figure 5.2: Output of solar PV

5.2.2 Direct Power Control

The direct power control strategy without PLL synchronization is designed based on the methodology presented. The performance of the technique is presented in Figure 5.3 to Figure 5.7.

The grid voltage produced is a perfect sinusoidal wave with the nominal frequency, and the outputs match their expected values in steady state. We also examine one cycle of the voltage waveform and confirm that the frequency of the signal is exactly 50 Hz as expected.
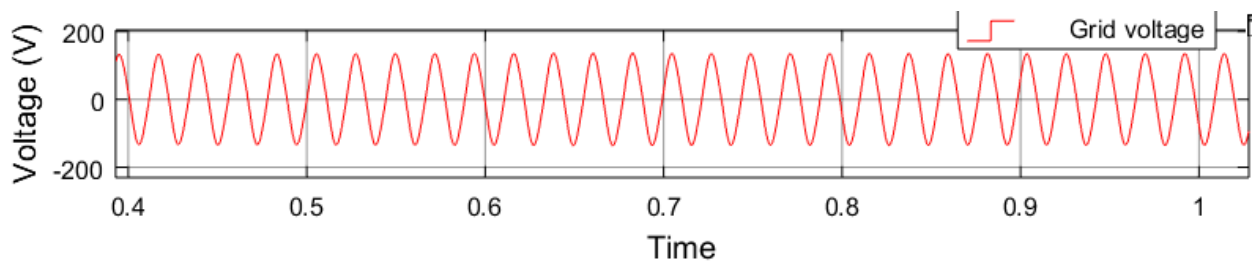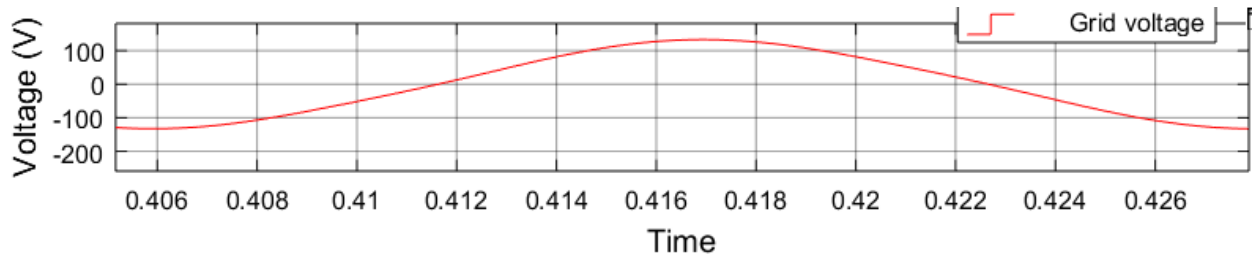

Figure 5.3: Output voltage

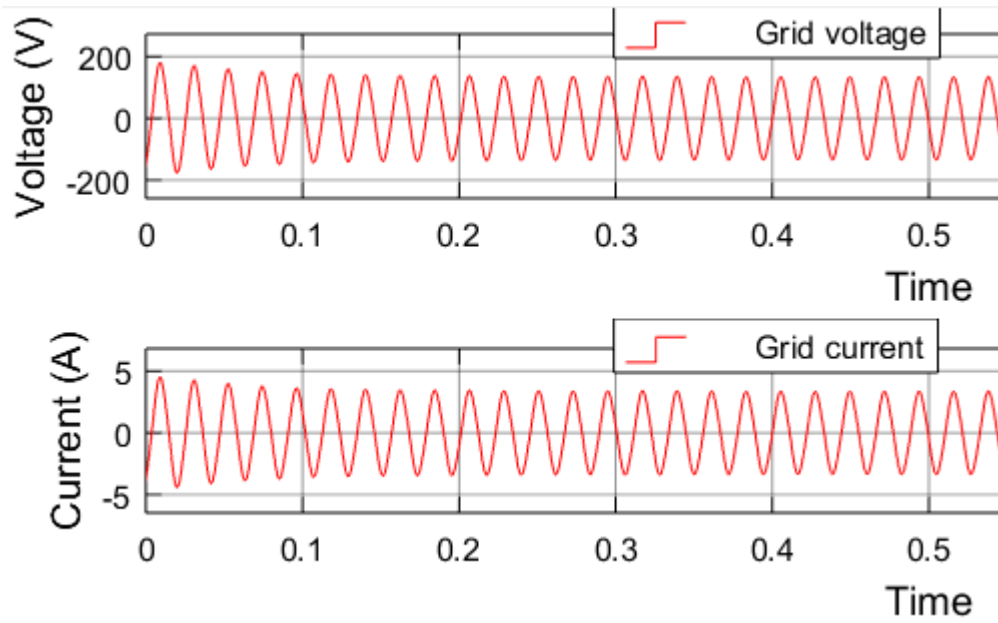Figure 5.4: One cycle of output voltage of inverter

Figure 5.5: Output voltage and current in phase

The transient response of the system is also observed. To simulate a line energization, a Breaker block is added to the model and the parameters are set as follows.

Table 5.2: Parameters for transient simulation

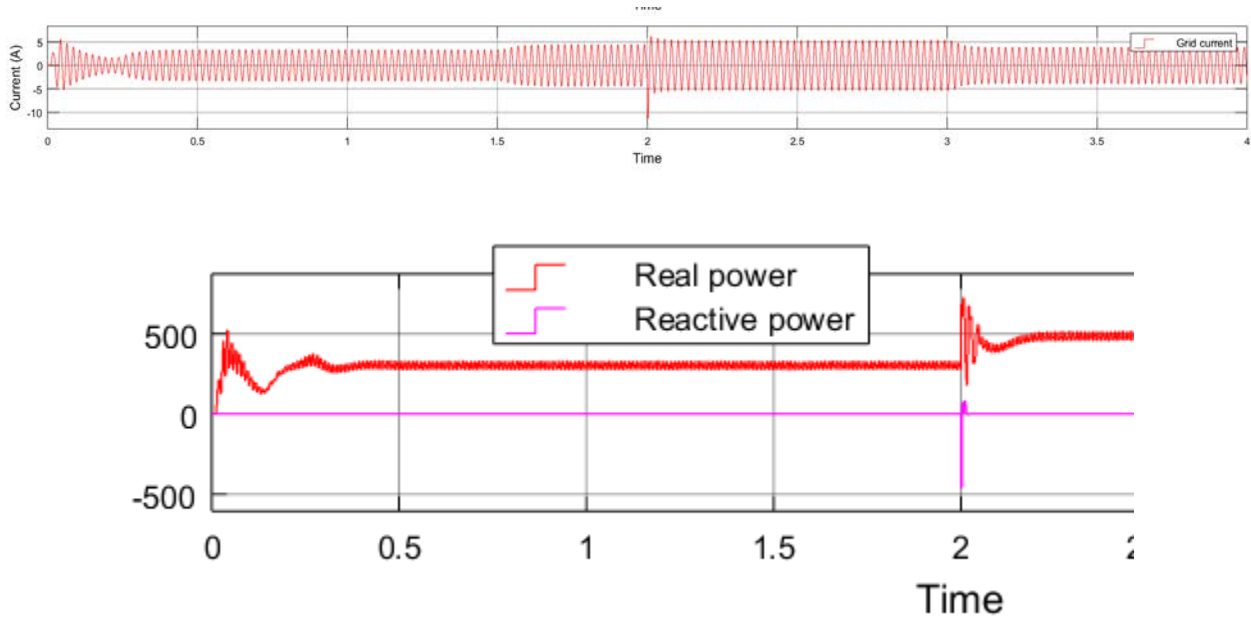| Breaker resistance (Ω)	0.01
Initial status	0 (open)
Snubber resistance (Ω)	1e8
Snubber capacitance (µF)	inf
Switching times	[2]

Figure 5.6: Response of PV system to transient

Once the transient is simulated by triggering the circuit breaker, a spike is observed in the current waveform and it returns to normal after a cycle. This shows that the settle time is less than 1.5ms (well within the desired range).
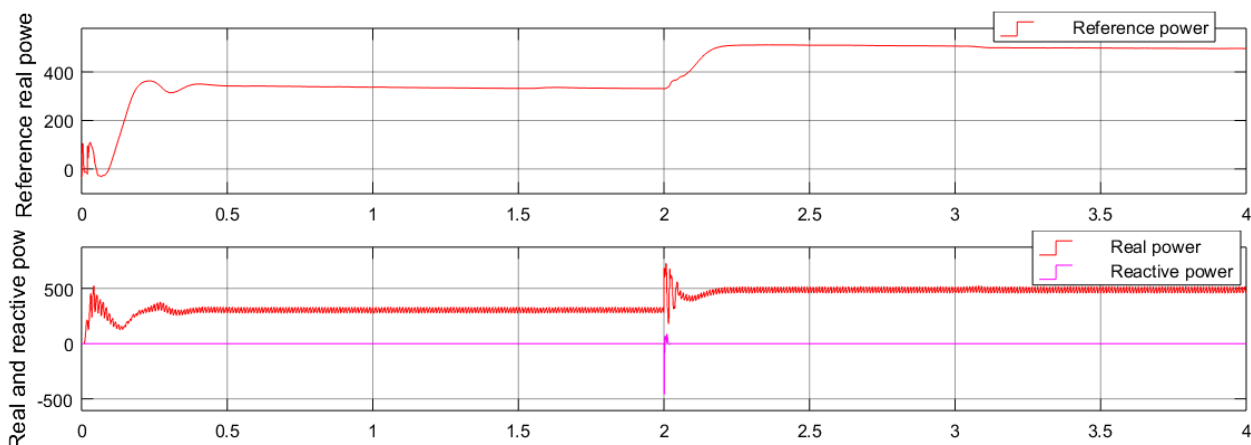
5.2.3 Real and Reactive Power Tracking

Figure 5.7: Real and reactive power tracking

The control strategy proposed demonstrates a fast, dynamic response and this results in the active power closely tracking the reference active power. Similarly, the control strategy is able to help achieve a unity power factor.
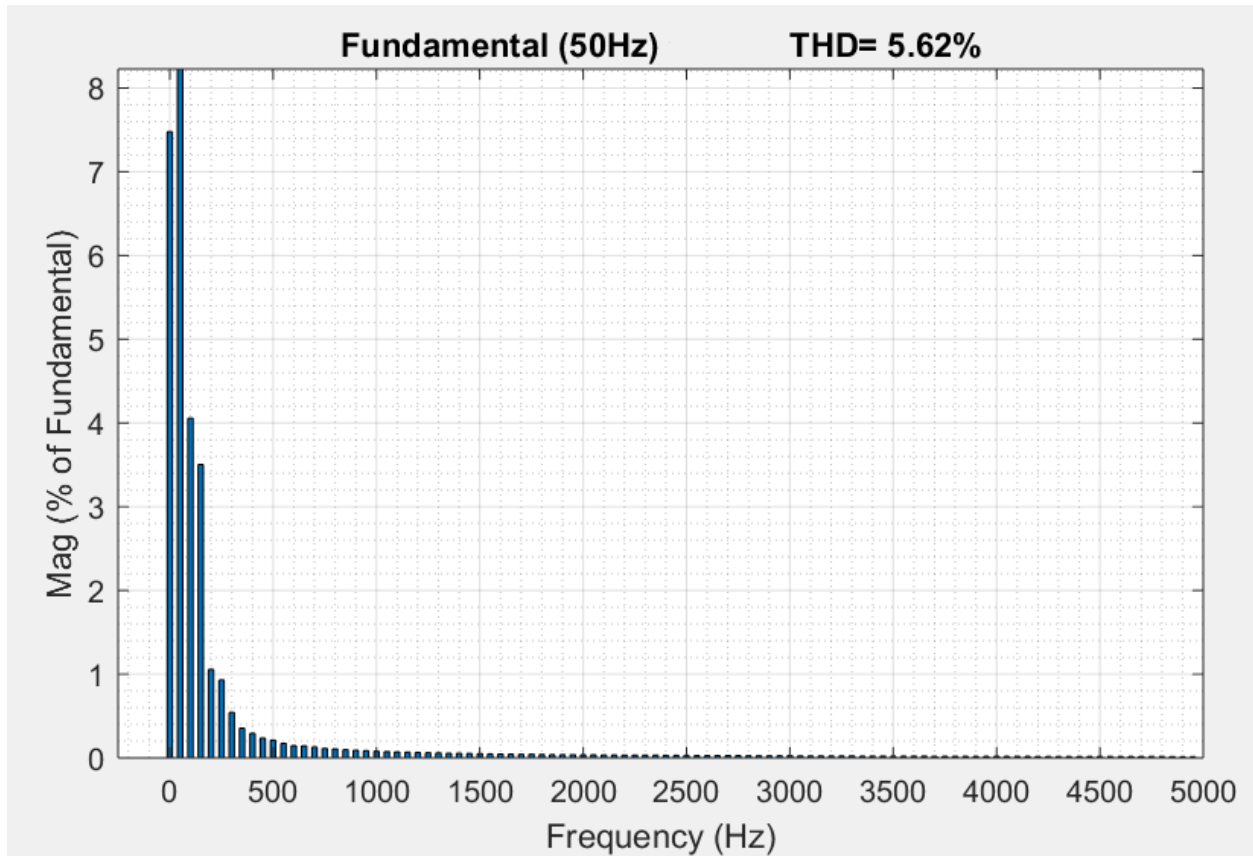

Figure 5.8: THD of the output voltage

The total harmonic distortion of the system is as shown in Figure 5.8.

5.2.4 SVPWM

The output voltage of the SVPWM technique implemented is shown. It is observed that this output voltage has the desired 5 levels and the waveform parallels a sinusoid. Because of the quality of the output, the size of the LC filter is relatively small.
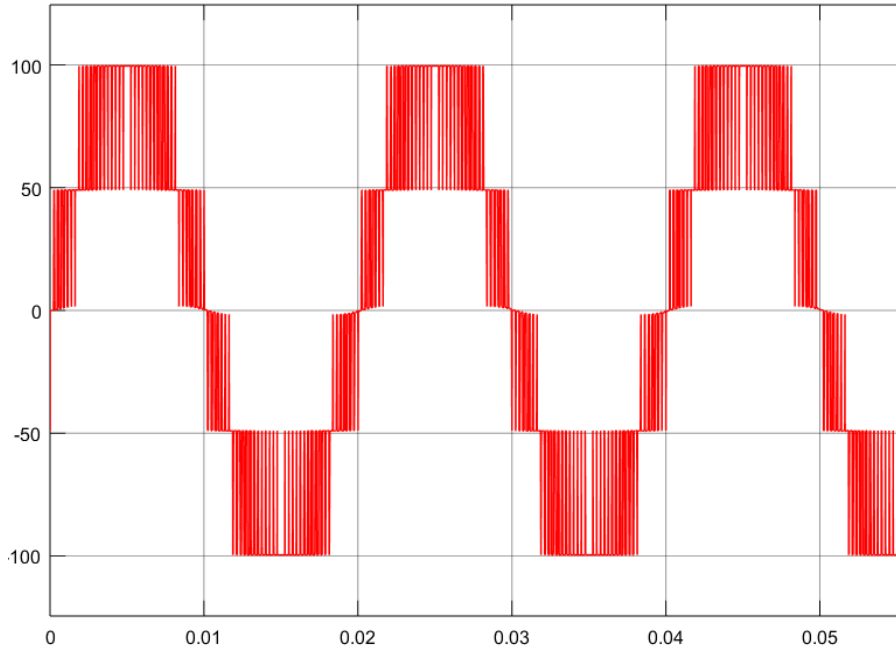
Figure 5.9: Output voltage of SVPWM

CHAPTER 6: CONCLUSIONS AND FUTURE WORK

6.1 Conclusions

This thesis details the direct power control strategy for single-phase, three-level, PV-connected system with the synchronization carried out without a PLL. The model is designed and simulated using MATLAB/Simulink and the results are analyzed. The performance of the proposed system is then examined and compared to conventional techniques. It is seen that the control system presented in this thesis can adequately control the voltage fed to the grid. The simulation carried out also shows excellent power control capabilities.

6.2 Future Work

This thesis explored the control strategies for single-phase, three-level grid-connected inverters and the simulation was carried out with a solar-PV source. In the future, other variable renewable energy sources such as wind and tidal energy can be modeled in MATLAB and used as the energy resource for simulating the system.

The direct power control (DPC) strategy was presented in this thesis. In the future, model predictive DPC, as well as other more sophisticated control strategies can be used for the modeling and simulation.

Apart from the transient fault conditions simulated in this thesis, the steady state and dynamic performance of the control strategy presented can be analyzed further by simulating more fault conditions.

References

[1] U.S. Energy Information Administration - EIA - Independent Statistics and Analysis https://www.eia.gov/tools/faqs/faq.php?id=427&t=3

[2] Explaining the plummeting cost of solar power, David Chandler- MIT News Office - http://news.mit.edu/2018/explaining-dropping-solar-cost-1120

[3] M. Monfared, M. Sanatkar, and S. Golestan, "Direct active and reactive power control of single-phase grid-tie converters," IET Power Electron., vol. 5, no. 8, pp. 1544, Sep. 2012.

[4] S. Golestan, M. Monfared, F. D. Freijedo, and J. M. Guerrero, "Dynamics assessment of advanced single-phase PLL structures," IEEE Trans. Ind. Electron., vol. 60, no. 6, pp. 2167-2177, Jun. 2013

[5] S. M. Silva, B. M. Lopes, B. J. C. Filho, R. P. Campana, and W. C. Bosventura, "Performance evaluation of PLL algorithms for single-phase grid-connected systems," in 39th Conf. Rec. IEEE IAS Annu. Meeting, pp. 2259-2263, 2004

[6] A. Luna, J. Rocabert, I. Candela, P. Rodriguez, R. Teodorescu and F. Blaabjerg, "Advanced structures for grid synchronization of power converters in distributed generation applications," 2012 IEEE Energy Conversion Congress and Exposition (ECCE), 2012.

[7] G. C. Hsieh, J. C. Hung, "Phase-locked loop techniques – A survey," IEEE Trans. On Ind. Electronics, vol.43, pp.609-615, Dec.1996

[8] Q. Zhong, P. Nguyen, Z. Ma, and W. Sheng, "Self-synchronized synchronverters: Inverters without a dedicated synchronization unit," IEEE Trans. Power Electron., vol. 29, no. 2, pp. 617-630, Feb. 2014

[9] M. Malinowski, M. Jasinski, and M. P. Kazmierkowski, "Simple direct power control of three-phase PWM rectifier using space-vector modulation (DPC-SVM)," IEEE Trans. Ind. Electron., vol. 51, no. 2, pp. 447-454, Apr. 2004

[10] J. Ma, W. Song, S. Jiao, J. Zhao, and X. Feng, "Power calculation for direct power control of single-phase three-level rectifiers without phase-locked loop," IEEE Trans. Industrial Electronics, vol. 63, no. 5, pp. 2871–2882, May 2016.

[11] Markvart, T., Ed., "Solar electricity", John Wiley & Sons, Chichester, U.K., 1994

[12] A. Nabae, I. Takahashi, H. Akagi, "A new neutral-point clamped PWM inverter," IEEE Transactions on Industry Applications, pp. 518-523, vol. IA-17, no.5, September/October 1981.

[13] Dolen, M. and Lorenz, R. D., "Industrially useful means for decomposition and differentiation of harmonic components of periodic waveforms". In Proceedings of the IEEE Industry Applications Society Annual Meeting, 2000, pp. 1016–1023.

[14] Begovic, M. M., Djuric, P. M., Dunlop, S. and Phadke, A. G., "Frequency tracking in power networks in the presence of harmonics", IEEE Transactions on Power Delivery, 8(2), April 1993, 480–486.

[15] Nedeljkovic, D., Nastran, J., Vocina, D. and Ambrozic, V. "Synchronization of active power filter current reference to the network". IEEE Transactions on Industrial Electronics, 46(2), April 1999, 333–339

[16] Sakakibara, Y. and Gleason, A., "Who is Fourier? A mathematical adventure, Language Research Foundation", Transnational College of Lex Tokyo, April 1995. ISBN 10: 0964350408.

[17] Mohan, N., Undeland, T., and Robbins, W., "*Power electronics: Converters, applications, and design",* 2nd ed., John Wiley & Sons, New York, 1995.